

The 18th Biennial Conference of International Society for Ecological Modelling

## Fully-Coupled Modeling of Shallow Water Flow and Pollutant Transport on Unstructured Grids

Shuangcai Li<sup>a\*</sup>, Christopher J. Duffy<sup>b</sup>

<sup>a</sup>*Risk Management Solutions, Inc., 7575 Gateway Blvd, Newark, CA 94560, USA*

<sup>b</sup>*Department of Civil and Environmental Engineering, Pennsylvania State University, University Park, PA 16802, USA*

---

### Abstract

Understanding the space-time dynamics of pollutant transport remains an essential impediment to accurate prediction of impacts on the ecology of rivers and coastal areas and also for establishing efficient strategies for pollution control and environmental protection. Numerical models are a powerful tool to study the water flows and pollutant transport, and recently a new generation of models is being developed to simulate the coupled flow and pollutant transport in shallow water. In this paper, a two-dimensional fully-coupled model of shallow water flows and pollutant transport was developed using a triangular unstructured grid (TIN: triangular irregular network), which is also an important module of the PIHM-Hydro modeling system. The model is based on a cell-centered upwind finite volume method using the HLL approximate Riemann solver. A multidimensional linear reconstruction technique and multi-dimensional slope limiter was implemented to achieve a second-order spatial accuracy. In order to make the model efficient and stable, an explicit-implicit method was used in temporal discretization by an operator splitting technique. A test case of the pollutant transport in a square cavity is used to validate the model. Then the model was further applied to two pollutant transport scenarios: microscale pollutant transport following dam break and mesoscale pollutant transport driven by storm surge in Galveston Bay. The numerical results show that the model could accurately predict the flow dynamics and pollutant transport in extreme events such as a dam break and a storm surge. According to the prediction of the model, the storm surge caused by the Hurricane Ike significantly extended the polluted area.

© 2011 Published by Elsevier B.V. Selection and/or peer-review under responsibility of School of Environment, Beijing Normal University.

*Keywords:* Shallow water flow; Transport; TIN

---

---

\* Corresponding author. Tel.: +1-814-321-3990.  
*E-mail address:* [lishuangcai@gmail.com](mailto:lishuangcai@gmail.com).

## 1. Introduction

Pollutant transport in rivers and coastal areas is a topic of increasing interest due to the increasingly severe pollution caused by construction projects, coastal defenses, discharge from industries and municipal facilities, flooding and radioactive waste disposal. This pollution may impair the ecology and environment and has potential to impact economy and human health. Understanding the dynamics of pollutants and their impacts on water quality is essential in accurate prediction of impacts on ecological system and establishing scientifically justified and practically efficient management strategy for pollution control and environmental protection. Numerical models are a powerful tool to study the water flows and pollutant transport.

In a two dimensional model, the shallow water equations are usually used to represent the fluid dynamics and the advection-diffusion equation is used for the pollutant transport. It is clear that the pollutant transport is determined by dynamics of water flow and the properties of the pollutant. In previous studies, it is common that the processes were decoupled based on the assumption that the dynamics of pollutants does not influence the flow behavior for low concentrations, and the non-conservative forms of equations were used by assuming the flow depth, velocities, and bed elevation vary smoothly in time and space [1]. These approaches are inappropriate and lead to inaccurate solution in some practical situations, e.g., when the flow changes fast in time and/or space. Therefore it is necessary to develop a fully coupled model in conservative form, which may avoid numerical instabilities in the pollutant concentration when applied to complex situations according to Murillo et al. [1]. This system can be treated as a hyperbolic system with the diffusion term as the source term.

It is challenging to numerically solve this kind of complex hyperbolic equations which are actually a system of coupled nonlinear partial differential equations. In many practical applications, a number of factors make the numerical solution even more difficult such as non-flat and rough bed, and complex domains. There have been numerous methods developed for solving the shallow water equations such as method of characteristics [e.g., 2], finite difference method [e.g., 3], finite element method [e.g., 1], and finite volume method [e.g., 4]. As for method of characteristics, it may not have solutions for all cases. Finite difference method has been widely used. However, it cannot guarantee strict conservation of mass and momentum, and only works on structured (often regular) grids. In practice, the complex domain boundary makes domain decomposition a major issue [5]. Compared to structured grids, unstructured grids can easily adapt to the complex geometry in real flow fields and is flexible to change the spatial resolution locally according to requirement, e.g., increasing the number of cells in regions of particular interest. Although finite element method has been used on unstructured grids, it may not work well when both subcritical and supercritical flows are encountered [2], and might produce solutions with local mass balance errors [6]. In contrast, finite volume method is characteristics of the local and global mass conservation property, the flexibility to apply to irregular domains and unstructured grids, and the reduced burden of explicit calculation memory requirement [7]. Therefore, finite volume method is used in this paper.

Recently several models were developed to simulate the coupled flow and pollutant transport in shallow water using finite volume methods. For instance, Murillo et al. [1] applied the first-order Roe's scheme to study the pollutant transport by shallow water flow in a small-scale test case without verification against the lab experiments or real flow field. Another drawback is this model is based on the Roe's scheme which is entropy-violating without entropy fix. Benkhaldoun et al. [3] used a well-balanced finite volume non-homogeneous Riemann solver (SRNH). The principal drawback of this method is that one parameter need be evaluated by some empirical equation and it is also difficult to implement compared to the traditional approximate Riemann solvers. To solve these problems in existing models, the objective of this paper is to develop a two-dimensional fully-coupled model of shallow water flows and

pollutant transport based on a cell-centered upwind finite volume method using the HLL approximate Riemann solver on unstructured triangular grids (TIN). Compared to the above methods, the HLL approximate Riemann solvers [8] modified by Toro [9] are robust and produce excellent results for a wide range of flow conditions [10]. It also avoids the entropy violating solution and explicitly includes the contact discontinuity which is ignored in other Riemann solvers except Osher's [11]. However, the HLL scheme is much simpler to implement compared to Osher's scheme. A multidimensional linear reconstruction technique and multi-dimensional slope limiter [12] is implemented to achieve a second-order spatial accuracy. The technique introduced by Bradford and Sanders [6] is adopted to mitigate the unbalanced approximation problems over bed slopes. In order to make the model efficient and stable, an explicit-implicit method is used in temporal discretization by an operator splitting technique, i.e., the advection part and non-stiff source terms are solved using explicit scheme while the diffusion term and the stiff source terms are handled by fully implicit scheme. In order to demonstrate its capability to provide accurate and efficient simulations for pollutant transport by shallow water flows, the model was applied to several test cases including advection of pollutant in a squared cavity, pollutant transport after an asymmetric dam break, and pollutant transport in Galveston Bay.

## 2. Methodology

### 2.1. Mathematical formulation

The model is represented by the two-dimensional shallow water equations coupled with the advection-dispersion equation for pollutant transport. The 2-D shallow water equations are derived from the Navier-Stokes equations by assuming negligible velocity change and hydrostatic pressure distribution in vertical direction, and incompressibility of water [e.g., 13; 14]. The shallow water equations written in conservative form are as follows:

$$\frac{\partial h}{\partial t} + \frac{\partial uh}{\partial x} + \frac{\partial vh}{\partial y} = S_p \quad (1)$$

$$\frac{\partial (uh)}{\partial t} + \frac{\partial (u^2h + gh^2/2)}{\partial x} + \frac{\partial (uvh)}{\partial y} = -gh(S_{ox} + S_{fx}) + f_cvh + \frac{1}{\rho} \left( \frac{\partial (hT_{xx})}{\partial x} + \frac{\partial (hT_{xy})}{\partial y} \right) + F_x \quad (2)$$

$$\frac{\partial (vh)}{\partial t} + \frac{\partial (uvh)}{\partial x} + \frac{\partial (v^2h + gh^2/2)}{\partial y} = -gh(S_{oy} + S_{fy}) - f_cuh + \frac{1}{\rho} \left( \frac{\partial (hT_{yx})}{\partial x} + \frac{\partial (hT_{yy})}{\partial y} \right) + F_y \quad (3)$$

In this two-dimensional model, the depth-averaged pollutant transport is of primary interest. The advection-dispersion equation is defined as:

$$\frac{\partial (\psi h)}{\partial t} + \frac{\partial (\psi uh)}{\partial x} + \frac{\partial (\psi vh)}{\partial y} = \frac{\partial}{\partial x} h \left( K_{xx} \frac{\partial c}{\partial x} + K_{xy} \frac{\partial c}{\partial y} \right) + \frac{\partial}{\partial y} h \left( K_{yx} \frac{\partial c}{\partial x} + K_{yy} \frac{\partial c}{\partial y} \right) + S_c \quad (4)$$

where  $t$  = time (T),  $x$  and  $y$  = horizontal coordinates (L),  $h$  = flow depth (L),  $u$  and  $v$  = depth-averaged flow velocity in  $x$ - and  $y$ -directions (L/T),  $\psi$  = depth-averaged volumetric pollutant concentration (L<sup>3</sup>/L<sup>3</sup>),

$g$  = gravitational acceleration ( $L/T^2$ ),  $S_{0x}$  and  $S_{0y}$  = bed slopes in x-and y-directions ( $L/L$ ),  $S_{fx}$  and  $S_{fy}$  = friction slopes in x-and y-directions ( $L/L$ ),  $K_{xx}$ ,  $K_{xy}$ ,  $K_{yx}$ , and  $K_{yy}$  = empirical dispersion coefficients accounting for turbulent diffusion and shear flow dispersion ( $L^2/T$ ),  $S_p$  = the additional source/sink including precipitation, infiltration etc.,  $S_c$  = the additional source/sink for the pollutant,  $T_{xx}$ ,  $T_{xy}$ ,  $T_{yx}$ , and  $T_{yy}$  = depth-averaged turbulent stresses,  $\rho$  = the water density,  $F_x$  and  $F_y$  = the additional forces arising from wind stress, tidal potential, atmospheric pressure etc.,  $f_c$  = the coefficient of the Coriolis force resulting from the earth's rotation ( $1/T$ ) which is calculated from:

$$f_c = 2\Omega \sin \varpi \tag{5}$$

where  $\Omega$  is the angular rotation rate of the Earth =  $\pi/12$  radians/hour, and  $\varpi$  is the latitude. The wind stress and the diffusion of momentum caused by turbulence and viscosity are neglected in this model.

$$\frac{\partial \mathbf{U}}{\partial t} + \frac{\partial \mathbf{E}}{\partial x} + \frac{\partial \mathbf{G}}{\partial y} = \mathbf{S} \tag{6}$$

Or conveniently it can be written as:

$$\frac{\partial \mathbf{U}}{\partial t} + \nabla \cdot \mathbf{F} = \mathbf{S} \tag{7}$$

where  $\mathbf{U}$  is the vector of the conservative variables,  $\mathbf{E}$  and  $\mathbf{G}$  are the flux vectors in x- and y-direction,  $\mathbf{S}$  is the vector of source terms,  $\mathbf{F} = (\mathbf{E}, \mathbf{G})^T$ .

$$\mathbf{U} = \begin{pmatrix} h \\ uh \\ vh \\ \psi h \end{pmatrix}, \mathbf{E} = \begin{pmatrix} uh \\ u^2h + gh^2/2 \\ uvh \\ \psi uh \end{pmatrix}, \mathbf{G} = \begin{pmatrix} vh \\ uv \\ v^2h + gh^2/2 \\ \psi vh \end{pmatrix}, \mathbf{S} = \begin{pmatrix} S_p \\ -gh(S_{ox} + S_{fx}) + f_cvh \\ -gh(S_{oy} + S_{fy}) - f_cuh \\ \nabla \cdot (\mathbf{K}h\nabla\psi) + S_c \end{pmatrix} \tag{8}$$

with the empirical dispersion matrix

$$\mathbf{K} = \begin{pmatrix} K_{xx} & K_{xy} \\ K_{yx} & K_{yy} \end{pmatrix} \tag{9}$$

Bed slope is calculated using

$$S_{0x} = \frac{\partial z}{\partial x} \text{ and } S_{0y} = \frac{\partial z}{\partial y} \tag{10}$$

There are several equations available for friction slope calculation such as Darcy-Weisbach equation for laminar flow and Manning equation for turbulent flow. Here the friction slope is estimated by the Manning equation:

$$S_{fx} = \frac{n^2 u \sqrt{u^2 + v^2}}{h^{4/3}} \quad (11)$$

$$S_{fy} = \frac{n^2 v \sqrt{u^2 + v^2}}{h^{4/3}} \quad (12)$$

with  $n$  = Manning coefficient.

The source term vector in the equations system (7) consists of three parts: bed slope  $\mathbf{S}_0$ , friction slope  $\mathbf{S}_f$  pollutant diffusion  $\mathbf{S}_d$ , and the additional source/sink term  $\mathbf{S}_p$ :

$$\begin{aligned} \mathbf{S}_0 &= (0 \quad -ghS_{0x} \quad -ghS_{0y} \quad 0)^T \\ \mathbf{S}_f &= (0 \quad -ghS_{fx} \quad -ghS_{fy} \quad 0)^T \\ \mathbf{S}_d &= (0 \quad 0 \quad 0 \quad \nabla \cdot (\mathbf{K}h\nabla\psi))^T \\ \mathbf{S}_p &= (S_p \quad f_c v h \quad -f_c u h \quad S_c)^T \end{aligned} \quad (13)$$

## 2.2. Domain decomposition

Quality unstructured grids are generated by the well known Triangle algorithm of Shewchuk [15]. Triangle allows the user to decompose the domain subject to constraints, such as boundaries, observation points, and/or nested multiresolution bathymetry [16].

## 2.3. Numerical model

Over each grid  $V_i$ , the system can be integrated as:

$$\int_{V_i} \frac{\partial \mathbf{U}}{\partial t} dV + \int_{V_i} \nabla \cdot \mathbf{F} dV = \int_{V_i} \mathbf{S} dV \quad (14)$$

Applying the Gauss theorem, the second integral on the left-hand side is replaced by a line integral around the control volume, which changes Equation (14) into:

$$\int_{V_i} \frac{\partial \mathbf{U}}{\partial t} dV + \oint_{\Gamma_i} \mathbf{F} \cdot \mathbf{n} d\Gamma = \int_{V_i} \mathbf{S} dV \quad (15)$$

with  $\Gamma$  = boundary of the control volume and  $\mathbf{n} = (n_x \ n_y)^T$  = the unit outward vector normal to the boundary.

A cell-centered finite volume method is formulated for Equation (15) over a Delaunay-type triangle-shaped control volume, where the dependent variables of the system are stored at the center of the control volume and represented as piecewise constant. The association of these variables with the centers enables the implementation of a high-order interpolation scheme [5]. Using the mid-point rule to Equation (15), it can be rewritten as:

$$\frac{\partial \mathbf{U}_i}{\partial t} = -\frac{1}{V_i} \sum_{j=1}^3 (\mathbf{F}_{ij} \cdot \mathbf{n}_{ij}) \Gamma_j + \mathbf{S}_i \tag{16}$$

with  $\mathbf{U}_i$  being the average values over the control volume  $V_i$ ,  $\mathbf{S}_i = \frac{1}{V_i} \int_{V_i} \mathbf{S} dV$  being the numerical

approximation of the source term,  $\mathbf{n}_{ij}$  being the unit outward normal vector to the edge  $j$ ,  $\mathbf{F}_{ij}$  is the numerical flux vector through the edge  $j$ , which is calculated using the HLL approximate Riemann solver. To solve the system in a fully-coupled mode using HLL scheme, the approach of Zoppou and Roberts [10] is followed to manipulate the flux terms. The rotation matrix is introduced:

$$\mathbf{T}_n = \begin{pmatrix} 1 & 0 & 0 & 0 \\ 0 & n_x & n_y & 0 \\ 0 & -n_y & n_x & 0 \\ 0 & 0 & 0 & 1 \end{pmatrix} \tag{17}$$

The application of this matrix aligns the normal  $\mathbf{n}$  with the  $x$ -axis. Using the rotational invariance property of the 2D shallow water equations, then:

$$\mathbf{F}(\mathbf{U}) \cdot \mathbf{n} = \mathbf{T}_n^{-1} \mathbf{E}(\mathbf{T}_n \mathbf{U}) \tag{18}$$

Applying Equation (18), Equation (15) becomes:

$$\int_{V_i} \frac{\partial \mathbf{U}}{\partial t} dV + \oint_{\Gamma_i} \mathbf{T}_n^{-1} \mathbf{E}(\mathbf{T}_n \mathbf{U}) d\Gamma = \int_{V_i} \mathbf{S} dV \tag{19}$$

Then Equation (16) becomes:

$$\frac{\partial \mathbf{U}_i}{\partial t} = -\frac{1}{V_i} \sum_{j=1}^3 \mathbf{T}_{n_{i,j}}^{-1} \tilde{\mathbf{E}}(\mathbf{T}_{n_{i,j}} \mathbf{U}_i, \mathbf{T}_{n_{i,j}} \mathbf{U}_j) \Gamma_j + \mathbf{S}_i \tag{20}$$

where  $\tilde{\mathbf{E}}$  is the numerical flux vector through the edge  $j$ .

It is noted that the solution for  $h$  and  $u$  is unaffected by  $v$  and  $\psi$ , the complete solution of the Riemann problem for the conservative quantities  $h$  and  $uh$  in the 2D shallow water equations is identical to that for the 1D ones [4; 10]. The following formulations are used to calculate the normal fluxes for the conservative variables  $h$  and  $uh$ , which are also the first two components of the numerical flux  $\tilde{\mathbf{E}}$ :

$$\tilde{\mathbf{E}}_{1,2}(\mathbf{U}_L, \mathbf{U}_R) = \begin{cases} \mathbf{E}_L & \text{if } S_L \geq 0 \\ \frac{S_R \mathbf{E}_L - S_L \mathbf{E}_R + S_R S_L (\mathbf{U}_R - \mathbf{U}_L)}{S_R - S_L} & \text{if } S_L \leq 0 \leq S_R \\ \mathbf{E}_R & \text{if } S_R \leq 0 \end{cases} \quad (21)$$

where  $\mathbf{U}_L = \mathbf{T}_{n_i,j} \mathbf{U}_i$  and  $\mathbf{U}_R = \mathbf{T}_{n_i,j} \mathbf{U}_j$ ,  $S_L$  and  $S_R$  are the wave speed estimates. Several formulations are available for calculation of  $S_L$  and  $S_R$ . The approach proposed by Toro [9] is used here:

$$S_L = \begin{cases} \min(u_L - \sqrt{gh_L}, u^* - \sqrt{gh^*}) & \text{if both sides are wet} \\ u_L - \sqrt{gh_L} & \text{if the right side is dry} \\ u_R - 2\sqrt{gh_R} & \text{if the left side is dry} \end{cases}$$

$$S_R = \begin{cases} \min(u_R + \sqrt{gh_R}, u^* + \sqrt{gh^*}) & \text{if both sides are wet} \\ u_L + 2\sqrt{gh_L} & \text{if the right side is dry} \\ u_R + \sqrt{gh_R} & \text{if the left side is dry} \end{cases} \quad (22)$$

$$u^* = \frac{1}{2}(u_L + u_R) + \sqrt{gh_L} - \sqrt{gh_R}$$

$$h^* = \frac{(u_L - u_R + 2(\sqrt{gh_L} + \sqrt{gh_R}))^2}{16g}$$

Finally, the normal flux for the conservative variable  $uh$  and  $\psi h$  are calculated from:

$$\tilde{\mathbf{E}}_3(\mathbf{U}_L, \mathbf{U}_R) = \begin{cases} \tilde{\mathbf{E}}_1 v_L & \text{if } u^* \geq 0 \\ \tilde{\mathbf{E}}_1 v_R & \text{if } u^* < 0 \end{cases} \quad (23)$$

And

$$\tilde{\mathbf{E}}_4(\mathbf{U}_L, \mathbf{U}_R) = \begin{cases} \tilde{\mathbf{E}}_1 \psi_L & \text{if } u^* \geq 0 \\ \tilde{\mathbf{E}}_1 \psi_R & \text{if } u^* < 0 \end{cases} \quad (24)$$

where  $E_1$  is the normal flux calculated using (5) for the conservative variable  $h$ .  $E_3$  and  $E_4$  are the third and fourth components of  $E(U_L, U_R)$  respectively.

#### 2.4. Linear reconstruction and multidimensional slope limiter

We attempt to preserve high spatial accuracy in the flow simulation by adopting a second order piecewise linear reconstruction. Jawahar and Kamath [12]'s multidimensional linear reconstruction techniques was adopted in this study. Compared to other multidimensional linear reconstruction techniques, this one uses a wide computational stencil and does not strongly depend on vertex values. It has also been shown that high order schemes may lead to nonphysical oscillatory solutions near discontinuities [9]. To avoid oscillations, we limit the solution slope during the linear reconstruction. The multidimensional slope limiter proposed by Jawahar and Kamath [12] has the advantages that: (1) the limiter is inherently multidimensional which fits unstructured grids, and (2) it is continuously differentiable.

#### 2.5. Source terms

The source term vector consists of bed slope, pollutant diffusion, and friction slope. It is of great importance to correctly treat the source terms in order to obtain accurate results.

##### 2.5.1. Bed slope

For the treatment of bed slope, there have been a few discussions in the literature [e.g., 14; 18; 19; 20; 21; 22]. In this paper, the triangular grids facilitate the computation of the bed slope. Denote  $(x_i, y_i, z_i)$  as local coordinates associated with vertex  $i$  of a certain triangle grid, where  $z_i$  is the bed elevation (Fig 2). The plane is defined by

$$\begin{vmatrix} x & y & z & 1 \\ x_1 & y_1 & z_1 & 1 \\ x_2 & y_2 & z_2 & 1 \\ x_3 & y_3 & z_3 & 1 \end{vmatrix} = 0 \quad (25)$$

Or  $z = ax + by + c$  in compact form with  $a$  and  $b$  = the coefficients. Now, the slopes of the triangular grid are simply calculated as:

$$S_{0x} = \frac{\partial z}{\partial x} = a = \frac{y_1(z_3 - z_2) + y_3(z_2 - z_1) + y_2(z_1 - z_3)}{x_3(y_1 - y_2) + x_1(y_2 - y_3) + x_2(y_3 - y_1)} \quad (26)$$

$$S_{0y} = \frac{\partial z}{\partial y} = b = -\frac{x_1(z_3 - z_2) + x_3(z_2 - z_1) + x_2(z_1 - z_3)}{x_3(y_1 - y_2) + x_1(y_2 - y_3) + x_2(y_3 - y_1)} \quad (27)$$

### 2.5.2. Diffusion source term

The integral of the diffusion term is modified by applying the Gauss theorem:

$$\int_{V_i} \nabla \cdot (\mathbf{K}h\nabla\psi) dV = \oint_{\Gamma_i} (\mathbf{K}h\nabla\psi) \cdot \mathbf{n} d\Gamma \quad (28)$$

This line integral is approximated by:

$$\oint_{\Gamma_i} (\mathbf{K}h\nabla\psi) \cdot \mathbf{n} d\Gamma = \sum_{j=1}^3 (\mathbf{K}h\nabla\psi)_{ij} \cdot \mathbf{n}_{ij} \Gamma_j \quad (29)$$

$(\mathbf{K}h\nabla\psi)_{ij}$  can be approached by:

$$(\mathbf{K}h\nabla\psi)_{ij} = (\mathbf{K}(\nabla\psi h - \psi\nabla h))_{ij} \approx \frac{\mathbf{K}_L + \mathbf{K}_R}{2} ((\nabla\psi h)_j - \min(\psi_L, \psi_R)(\nabla h)_j) \quad (30)$$

where  $(\nabla\psi h)_j$  and is the face gradient calculated during the linear reconstruction.  $h$  is evaluated as  $\min(\psi_L, \psi_R)$  in order to avoid diffusion in dry/wet edges.

### 2.5.3. Friction source term

Friction slope is discretized in a point-wise manner, say, evaluated at the centroid.

### 2.6. Time integration

If a purely explicit scheme is used to solve the equations system (20), the stability is determined by the combination of advection and diffusion. It is well known that the time step is restricted by Courant–Friedrichs-Lewy (CFL) number and the Peclet ( $Pe$ ) number, so that

$$CFL + Pe \leq 1 \quad (31)$$

with

$$CFL = \frac{2 \max(\left(\sqrt{u^2 + v^2} + c\right)_i)}{\min(d_i)} \Delta t_{CFL} \quad (32)$$

$$Pe = \frac{\max(\mathbf{K} * \mathbf{n})_{i,j}}{2 \min(l_i^2)} \Delta t_{Pe} \quad (33)$$

where  $i$  is the cell index and  $j$  denotes the edge,  $d_i$  represents the whole set of distances between the  $i$ th centroid and the those of its neighboring cells, and  $l_i = \min(V_i / \Gamma)_j$ .

In order to reduce the numerical instabilities related to the friction slope when the water depth is very small and circumvent the time constraint by Peclet number, a semi-implicit method is used. The system can be split into two ordinary differential equations:

$$\frac{\partial \mathbf{U}_i}{\partial t} = -\frac{1}{V_i} \sum_{j=1}^3 (\mathbf{F}_{ij} \cdot \mathbf{n}_{ij}) \Gamma_j + \mathbf{S}_{0i} \quad (34)$$

$$\frac{\partial \mathbf{U}_i}{\partial t} = \mathbf{S}_{fi} + \mathbf{S}_{di} \quad (35)$$

The right hand side (RHS) of Equation (34) consists of advection and bed slope source term while the RHS of Equation (35) includes friction slope and pollutant diffusion source terms. In the first step, Equation (34) is solved by an explicit method as described below. In next step, using the values obtained from the first step as the initial conditions, Equation (35) is solved using an implicit method (BDF) provide by an advanced ODE solver CVODE [23].

The explicit time integration is performed by the first-order Euler method or a total variation diminishing (TVD) Runge-Kutta method [24] which has been used in many literatures thanks to its stability and high-order accuracy (third-order):

$$\begin{aligned} \mathbf{U}_1 &= \mathbf{U}^n + \Delta t f(\mathbf{U}^n) \\ \mathbf{U}_2 &= \frac{3}{4} \mathbf{U}^n + \frac{1}{4} \mathbf{U}_1 + \frac{1}{4} \Delta t f(\mathbf{U}_1) \\ \mathbf{U}^{n+1} &= \frac{1}{3} \mathbf{U}^n + \frac{1}{3} \mathbf{U}_2 + \frac{2}{3} \Delta t f(\mathbf{U}_2) \end{aligned} \quad (36)$$

where  $f$  is the right hand side of Equation (34).

The explicit time integration is performed by the first-order Euler method or a total variation diminishing (TVD) Runge-Kutta method [24] which has been used in many literatures thanks to its stability and high-order accuracy (third-order):

Since the explicit scheme is only applied to advection, the time step is limited by  $CFL$  condition. Therefore, an adaptive  $\Delta t$  is used in the model according to the formula

$$\Delta t \leq \frac{\min(d_i)}{2 \max\left(\left(\sqrt{u^2 + v^2} + c\right)_i\right)} \quad (37)$$

### 2.7. Boundary conditions

Two types of boundaries, open boundary and solid wall boundary, are considered in the model. Details of their implementation were discussed in Li and Duffy [16].

## 3. Results and discussion

In order to test the stability and accuracy of the model, it has been applied in three test cases. The first one solves a pollutant transport in a square cavity, which is used to validate model in simulating pollutant advection. The second test case involves a microscale pollutant transport scenario following an asymmetric dam break. The objective of this test case is to test the ability of the model in prediction pollutant transport by shocks or sharp fronts under different magnitude of diffusion. The third one is a mesoscale application, i.e., modeling pollutant transport by tidal flow and storm surge in Galveston Bay off the coast of Texas during hurricane Ike.

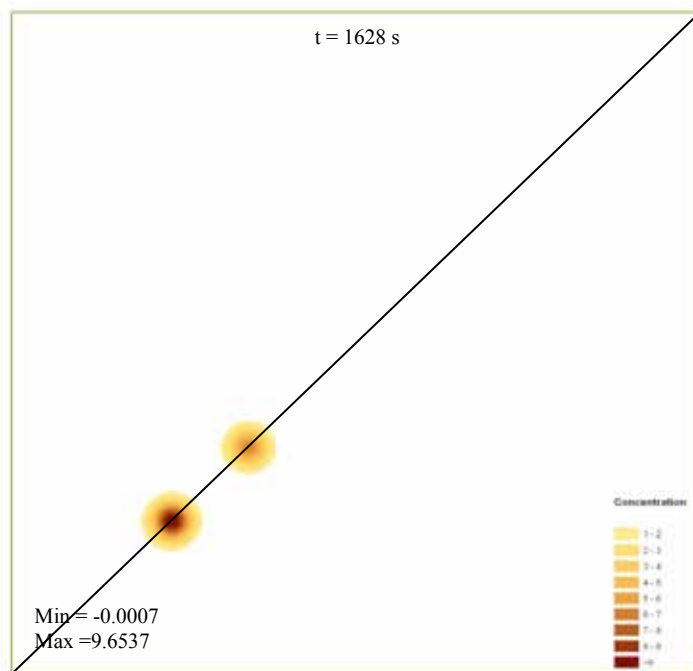
### 3.1. Advection of pollutant in a square cavity

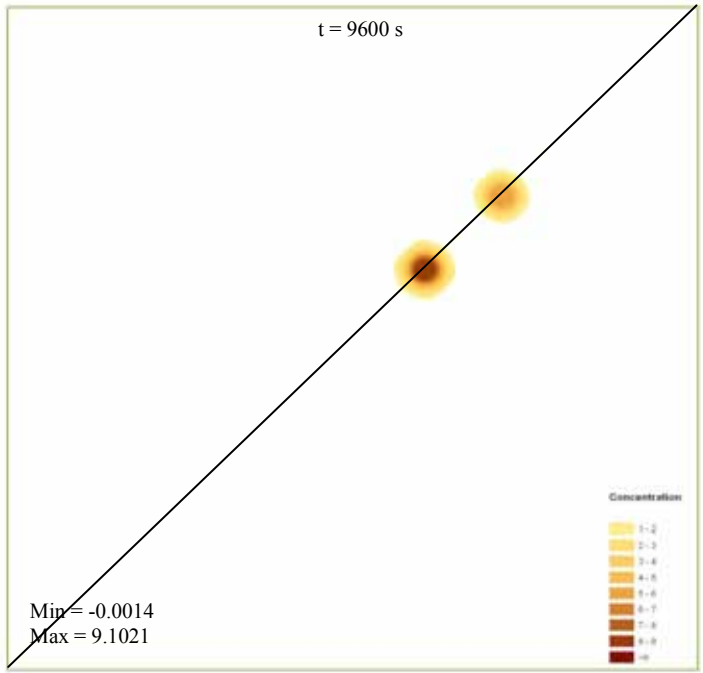
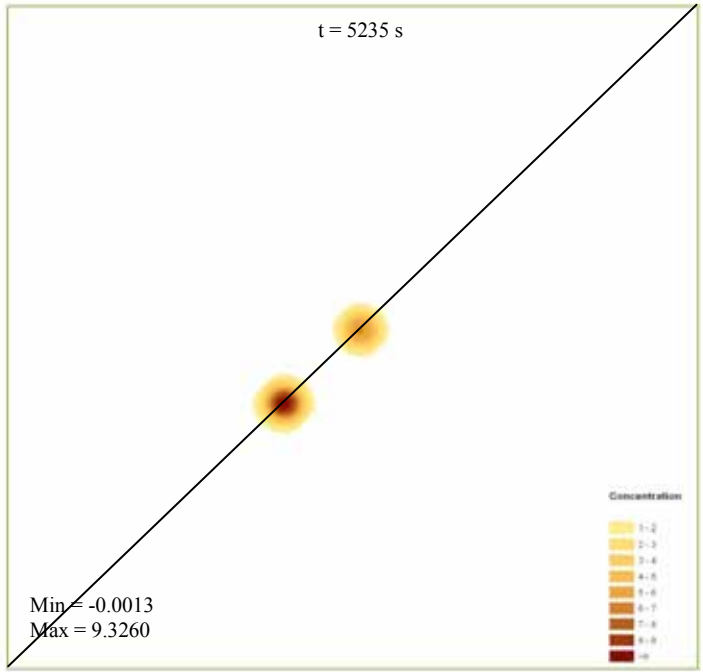
The first example is about the advection-dominant pollutant transport ( $\mathbf{K} = \mathbf{0}$ ) in a square cavity with smooth topography [25], which is used to validate the model. The computational domain is a 9 kilometer by 9 kilometer square channel with the Manning's roughness of  $0.025 \text{ s/m}^{1/3}$  and the bed slope  $S_{0x} = S_{0y} = -0.001$ . The domain was decomposed into 85264 triangles. Initially, the uniform flow conditions were imposed on the whole domain, i.e.,  $u = v = 0.5 \text{ m/s}$  and  $h = 0.2485 \text{ m}$ . The initial pollutant concentration was given by the superposition of two Gaussian distribution:

$$\psi(0, x, y) = \psi_1 \exp\left(-\frac{(x-x_1)^2 + (y-y_1)^2}{\delta_1^2}\right) + \psi_2 \exp\left(-\frac{(x-x_2)^2 + (y-y_2)^2}{\delta_2^2}\right) \quad (38)$$

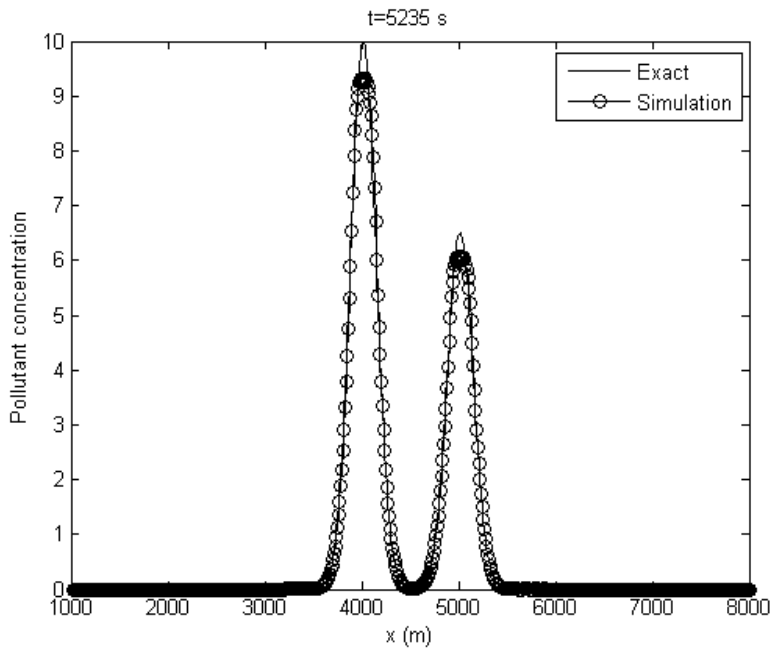
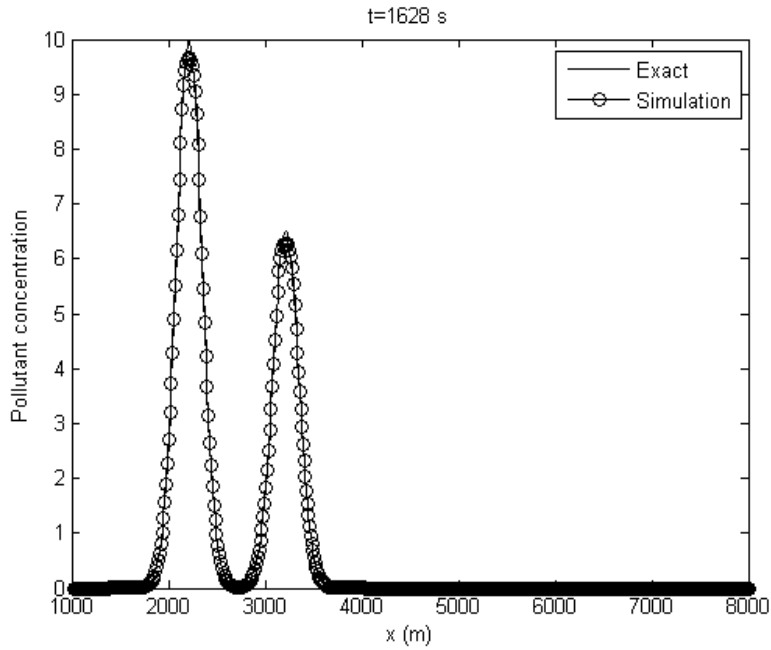
with  $x_1 = y_1 = 1400$  m, and  $x_2 = y_2 = 2400$  m,  $\psi_1 = 10$  and  $\psi_2 = 6.5$ , and  $\delta_1 = \delta_2 = 264$ . The free outfall or transmissive flow conditions were applied at all the boundaries. Analytically the pollutant concentration moves along the diagonal ( $x = y$ ) of the domain at the constant speed  $u = v = 0.5$  m/s with its shape preserved.

Fig. 1 shows the contour maps of pollutant concentration at three simulation times  $t = 1628$ , 5235, and 9600 s. The profiles of pollutant concentration are given in Fig. 2. Close examination of the results indicates that the shape of pollutant plume was preserved fairly well. A further comparison with the published simulations of SRNH [26] demonstrates the performance of this model is satisfactory with the error of -9.0% for the maximum concentration (Table 1). The accuracy of this model is almost same with that of SRNH on the fixed meshes. The advantage of this model is that it is easy to implement. The numerical results, however, are still affected by numerical diffusion as the simulation time increases. Overall, this simulation is convincing confirmation of the model's ability to predict advection of pollutant by shallow water flow.





Spatial distributions of pollutant concentration over the square cavity at three simulation times



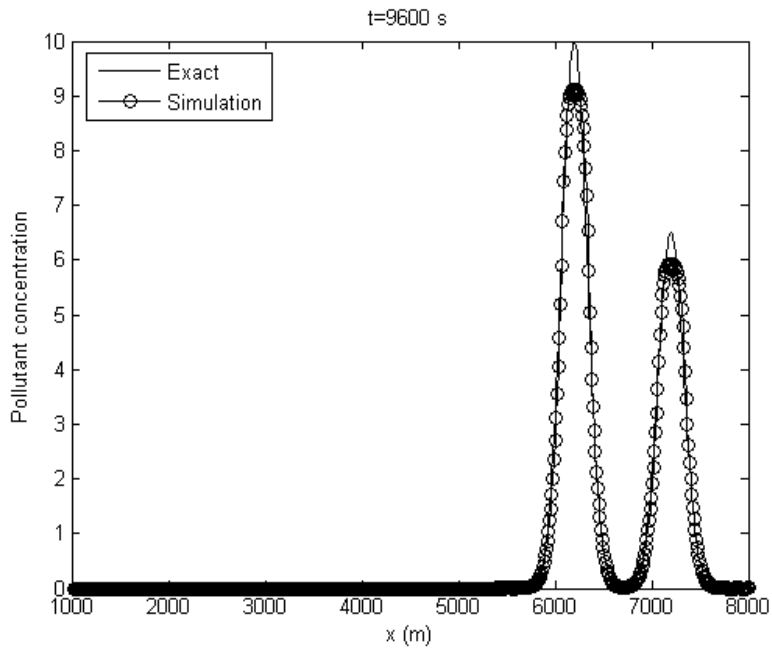


Fig. 2. Pollutant concentrations along the diagonal of the square cavity at three simulation times

Table 1. Comparison of this model with the exact solutions and the SRNH scheme with Van Albada limiter for the pollutant transport in a square cavity at  $t = 9600$  s

	Exact	SRNH	Model
# of elements		85504	85264
# of nodes		43073	42749
Minimum of concentration	0.0	-0.0054	-0.0014
Maximum of concentration	10.0	9.12 (-8.8%)	9.10 (-9.0%)

### 3.2. Pollutant transport following an asymmetric dam break

This is a microscale test case used to demonstrate the capability of the model in predicting pollutant transport by shocks or sharp fronts under different magnitude of diffusion. This example was adapted from Murillo et al. [1]. The laboratory set-up plan view is shown in Fig. 3 with flat bed ( $S_{0x} = S_{0y} = 0$ ) and a Manning roughness of  $0.01 \text{ s/m}^{1/3}$ . The computational domain was decomposed into 2330 triangles. Initially the flow depth was set to 0.5 m and 0.1 m respectively at the lower and upper half which were separated by a gate (dam) shown in Fig. 3. Flow velocities were set to zero. The initial concentration is a circular step distribution around the gate, defined as:

$$\psi(x, y, 0) = \begin{cases} 2 & \text{if } r \geq r_0 \\ 1 & \text{if } r < r_0 \end{cases} \text{ with } r = \left( (x - 1.97)^2 + (y - 1.35)^2 \right)^{1/2} \text{ and } r_0 = 0.65 \text{ m} \quad (39)$$

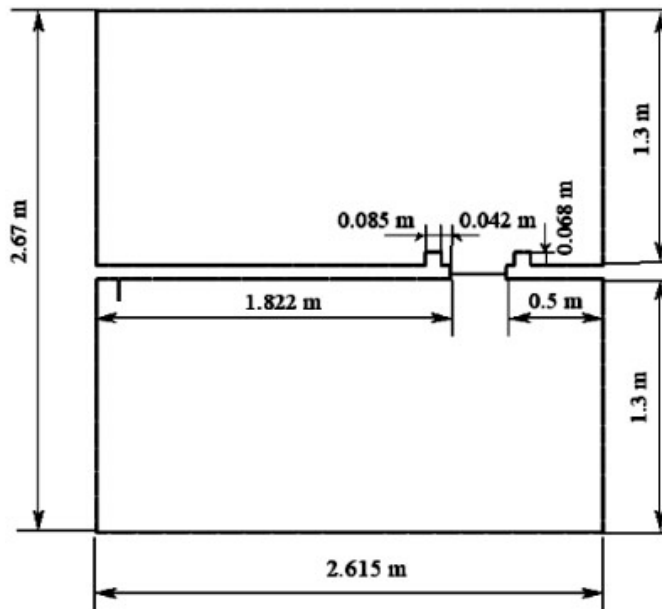


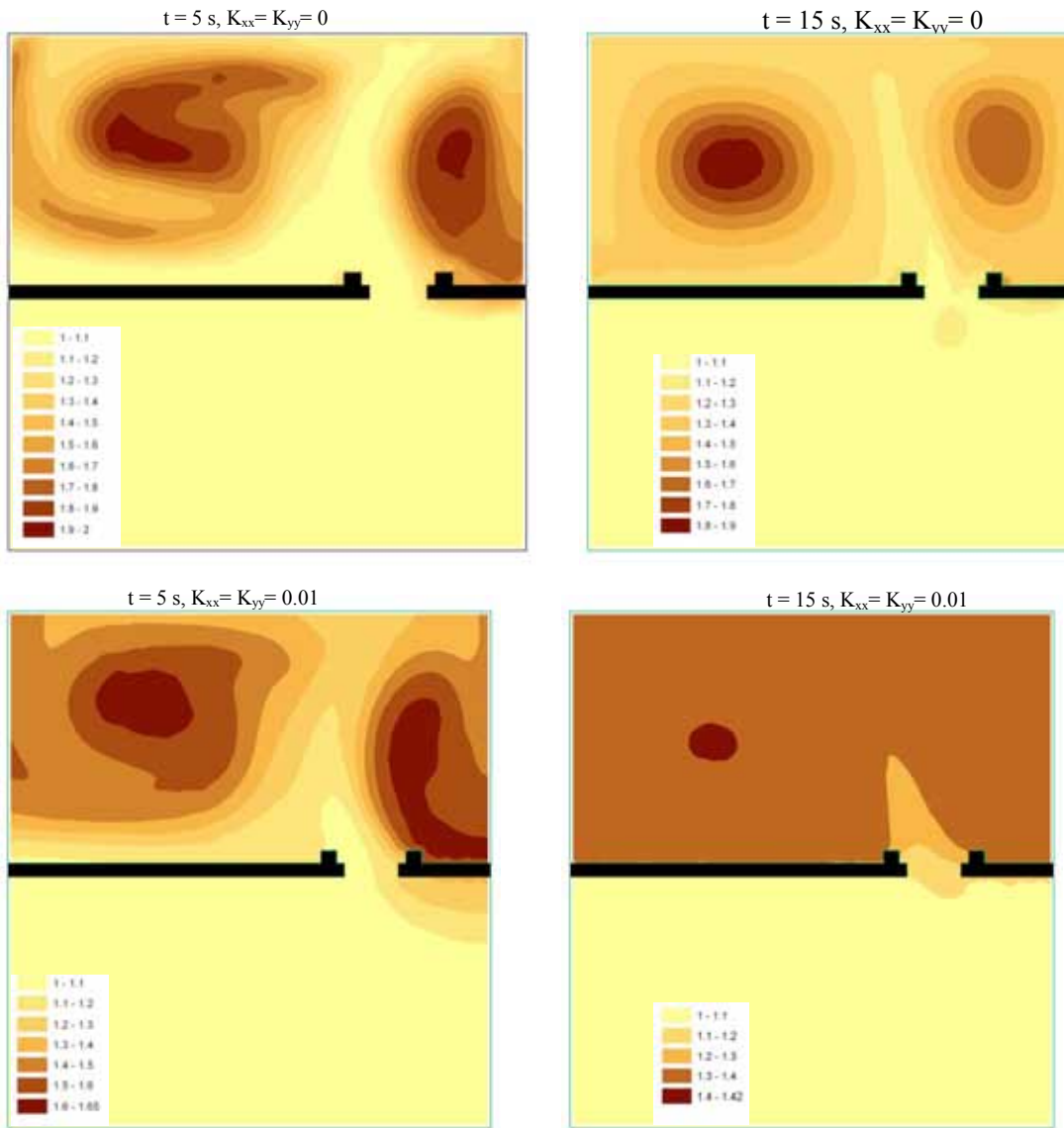
Fig. 3. Plan view of the laboratory set-up of the asymmetric dam break experiment (from Murillo et al. [1]).

Three numerical experiments were conducted with different dispersion coefficients: (1)  $\mathbf{K} = \begin{pmatrix} 0 & 0 \\ 0 & 0 \end{pmatrix}$ ,

(2)  $\mathbf{K} = \begin{pmatrix} 0.01 & 0 \\ 0 & 0.01 \end{pmatrix}$ , and (3)  $\mathbf{K} = \begin{pmatrix} 1 & 0 \\ 0 & 1 \end{pmatrix}$ . Fig. 4 shows the numerical results. In the advection-

dominant case (e.g.,  $\mathbf{K} = \mathbf{0}$ ), the pollutant concentration varies remarkably across the domain. At  $t = 15 \text{ s}$ , the concentration varies from 1 to 1.9. In the second experiment, the dispersion effect is included. The spatial variations of pollutant concentration diminished. In the third test case where the dispersion was dominant, the pollutant concentration is almost same across the domain in a short period of time, say,  $t =$

5 s. One advantage of this model is that the time step is not restricted by the Peclet number by implicit treatment of the diffusion term.



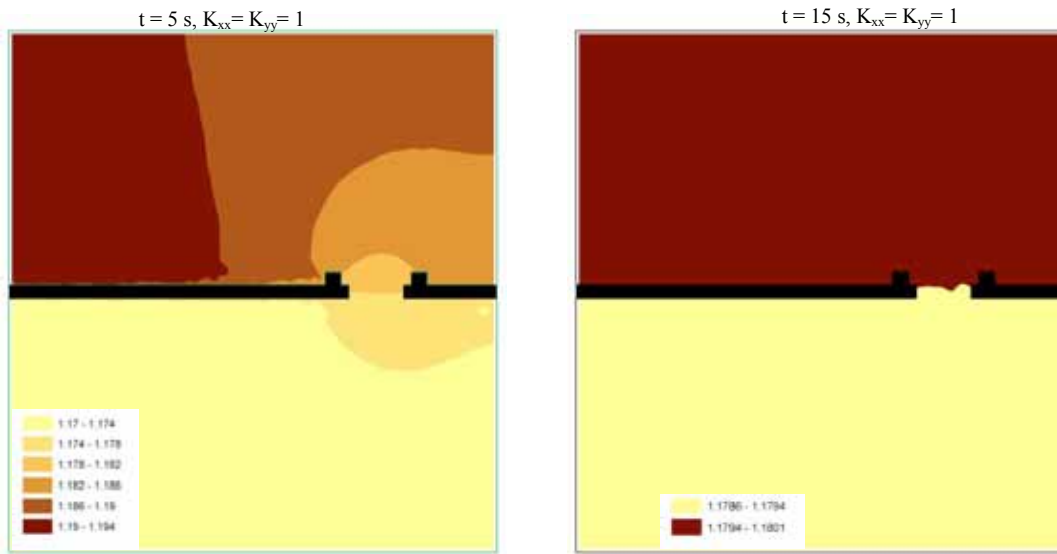


Fig. 4. Spatial distribution of pollutant concentration following an asymmetric dam break under different magnitude of dispersion

### 3.3. Pollutant transport in Galveston Bay

This test case involves a contamination scenario in Galveston Bay of Texas, which connects the Port of Houston and the Gulf of Mexico. It is used to demonstrate the capabilities of the model in predicting the mesoscale flow and pollutant dynamics driven by a storm surge and tidal flow. The area of the bay is about 2805 km<sup>2</sup> and its bathymetry is shown in Fig. 5. The domain is quite complicated with respect to both geometry and topography. There are 17 islands included in the domain, and the bathymetry varies from very deep in the coastal area and the Houston ship channel to very shallow within the bay.

The domain is decomposed into 3397 triangles (Fig. 5) with the structure slightly different from the one used in Aizinger and Dawson [27]. Following Aizinger and Dawson [27], the bottom friction coefficient was set as 0.004. The Coriolis parameter was 7.07E-5 according to Equation (5). The solid wall boundary condition was imposed on the land and island boundaries. An open boundary condition was applied at the interface between the bay and the Gulf of Mexico as shown in Fig. 5. The measured tidal data from 0:00 of September 1 to 19:00 of September 15, 2008 (local time) at the Galveston Pleasure Pier, TX (<http://tidesandcurrents.noaa.gov/>) was used. The tidal elevations were influenced by Hurricane Ike during September 12 and 13 as can be observed in Fig. 6. It is also noted that there were several unusually high spikes on September 8, 9 and 15 with very short duration, which may be caused by the measurement errors. At 19:00 of day 6, a pollutant source was placed at a point (3.28E+5, 3.25E+6) meters of the ship channel, with a steady rate of 500 m<sup>3</sup>/s.

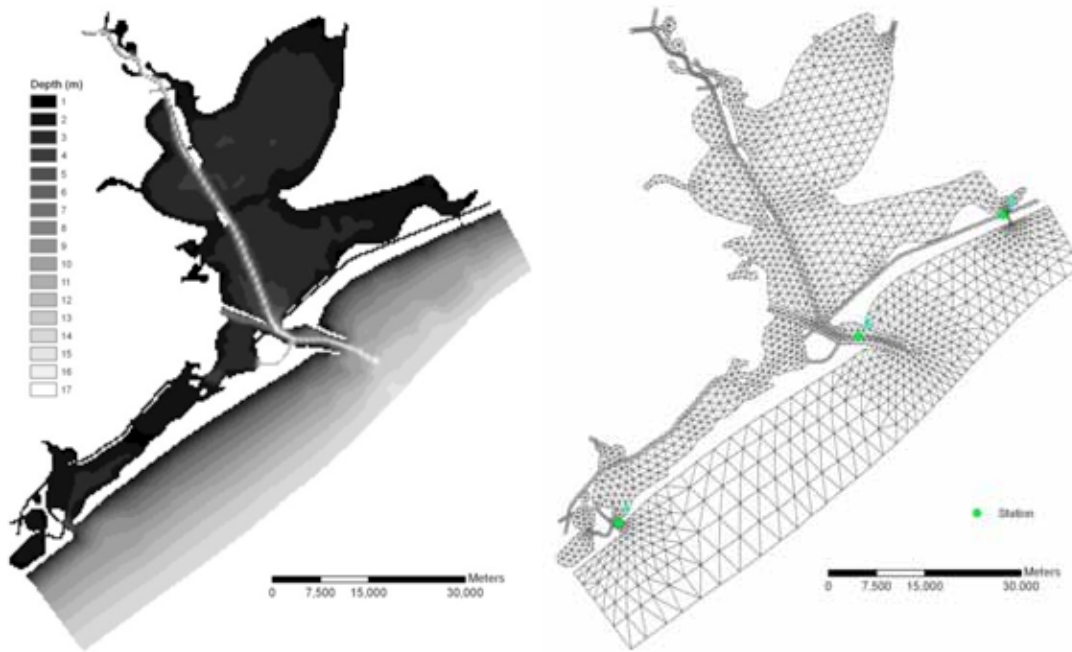


Fig. 5. The bathymetry (left) and computational mesh (right) of the Galveston Bay. The green points represent three stations where the simulation is done.

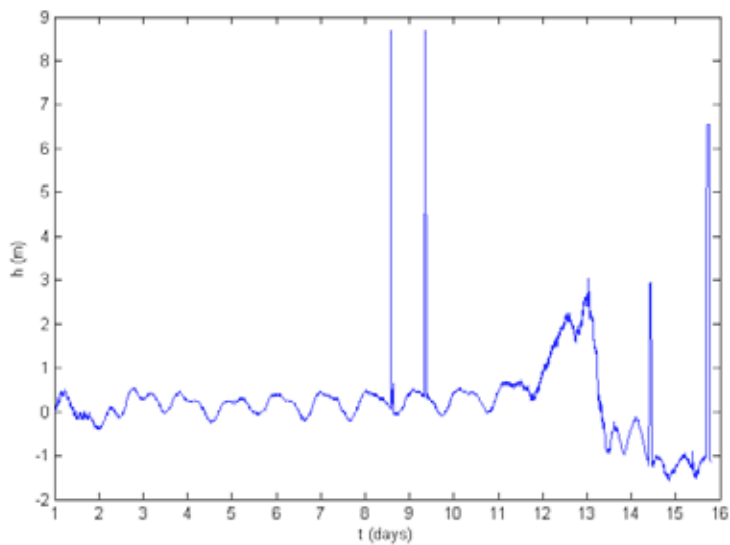


Fig. 6. Time series of water elevations at the open boundary. Note that the spikes are measurement errors since the NOAA tide gauge data was not verified at the time the model was developed and were not removed for the simulation

Fig. 7 shows the predicted elevations and pollutant concentration from day 6 to day 15 at three locations, Station 1 ( $2.94\text{E}+5$ ,  $3.22\text{E}+6$ ), Station 2 ( $3.31\text{E}+5$ ,  $2.25\text{E}+6$ ), and Station 3 ( $3.53\text{E}+5$ ,  $3.27\text{E}+6$ ) meters (Fig. 5). Station 1 is located at the narrow inlet from the Gulf in the bottom left of the domain. Station 2 is at the inlet in the deep ship channel from Gulf to the Galveston Bay. Station 3 is located at a shallow narrow channel within the bay in the bottom right of the domain. The results indicate a phase lag of approximately 1.2 hours between the open boundary and the three locations, which is consistent to the observations by NOAA (<http://tidesandcurrents.noaa.gov/>). The phase lags between these three stations are negligible which are reasonable based on the uniform boundary conditions and the similar distances between the open boundary and the station.

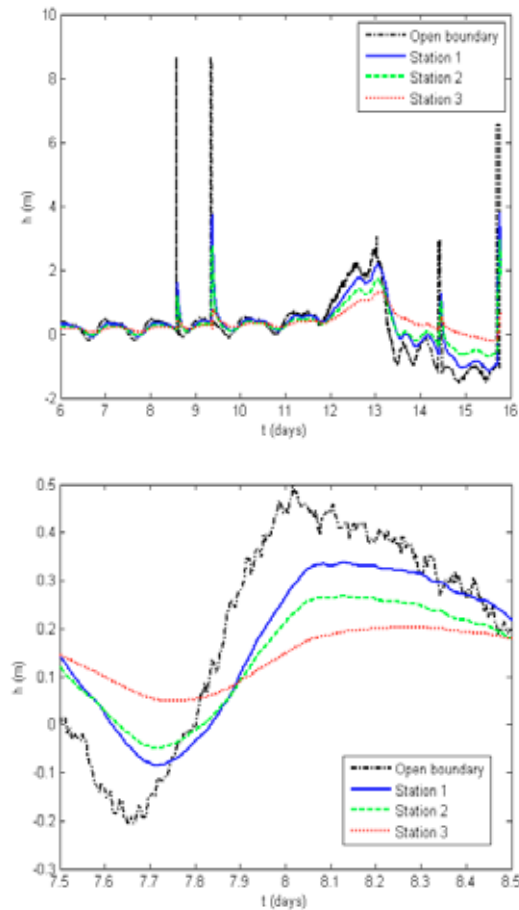
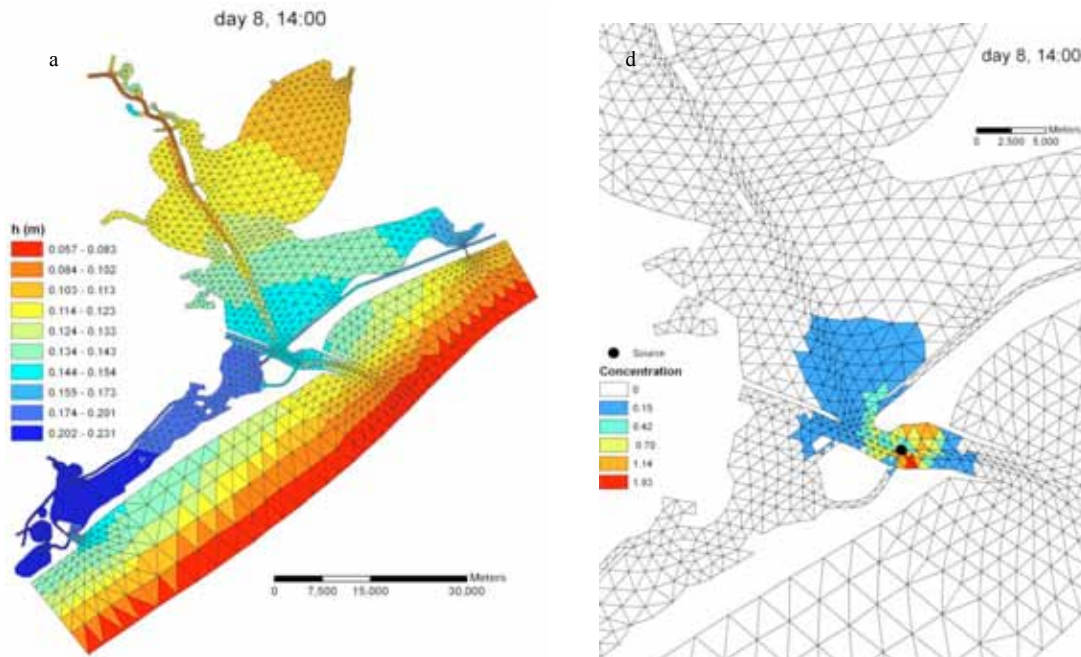


Fig. 7. Time series of predicted water elevations from day 6 to day 15 (left) at the 3 stations. The zoom-in figure on the right shows the temporal variation of water surface elevations in 1 day.

Additional insight into the flow dynamics is gained by considering the spatial distribution of water surface elevation and pollutant over the entire domain. Fig. 8 (a), (b) and (c) show three snapshots of the water surface elevations at different computational times. Fig. 8 (a) shows the middle of an ebb tide. The tides are relatively low out in the Gulf, somewhat higher in the middle part of the bay, and even higher in bottom left of the bay which is due to the narrow outlets to the other parts of the bay and the Gulf. The

variation in tidal amplitude becomes fairly small within the bay. Fig. 8 (b) and (c) are two snapshots of the tidal elevation at the middle and peak of a flood tide during the Hurricane Ike. The tidal waves were still progressing up into the bay, with the water surface elevation much higher than normal tidal cycles. As can be observed in Fig. 8 (c), the water surface elevations were between 0.5 m to 1 m in most parts of the bay.

Corresponding to the times for the figures on the left of Fig. 8, three snapshots are shown on the right to demonstrate the spread of pollutant caused by tidal flow. It is easy to see that the storm surge caused by the Hurricane Ike significantly extended the polluted area. The comparison between the polluted area before the Hurricane (Fig. 9 (a)) and after (Fig. 9 (b) and (c)) indicates the storm surge propagated the pollutant much deeper into the Bay and out to the Gulf. The experiment shows that the model is very stable and robust in simulating the mesoscale flow dynamics and pollutant transport driven by storm surge.



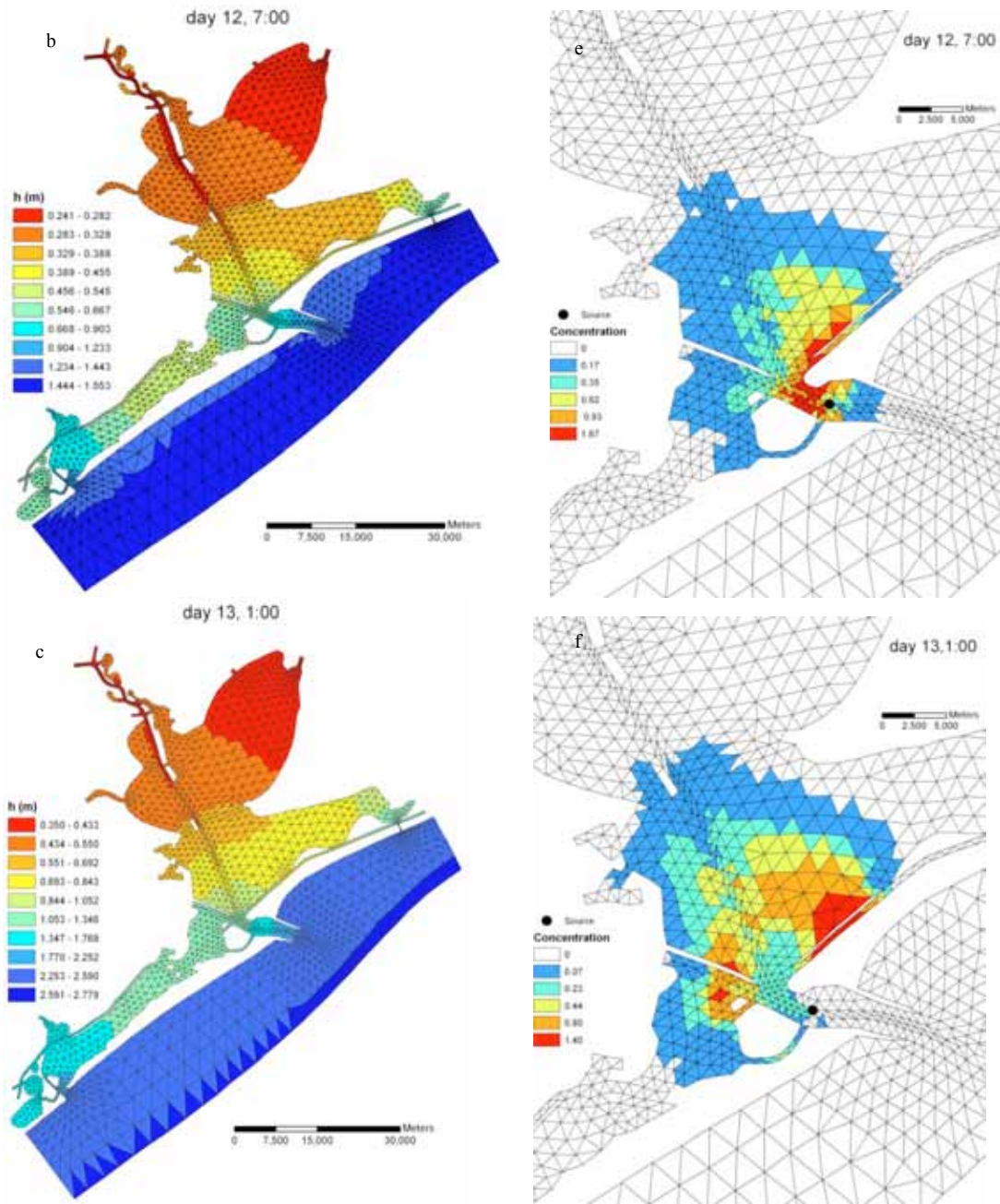


Fig. 8. Spatial distribution of predicted water elevations (left) and pollutant concentrations (right) over Galveston Bay at 3 computational times as indicated, i.e., before the storm surge and during storm surge.

#### 4. Conclusions

In this study, a fully-coupled model of shallow water flow and pollutant transport was developed as an important module of PIHM-Hydro and tested over a range of physical and numerical conditions. The model is based on a cell-centered upwind finite volume method using the HLL approximate Riemann solver. The multidimensional linear reconstruction technique and multi-dimensional slope limiter were also used here to achieve a second-order spatial accuracy.

The advantages of this model are that (1) it is capable of accurately simulating the pollutant transport by shallow water flow by fully coupling these processes physically and numerically; and (2) the time step is not restricted by the Peclet number by implicit treatment of the diffusion term. As a module of the PIHM-Hydro modeling system, this model also shows its advantages in terms of handling complicated geometry by using the Delaunay triangulation based on Shewchuk's algorithm, and producing accurate and stable solutions over a wide range of spatial scales and hydrological events such as dam break and storm surge stably by using the approximate Riemann solver and the semi-implicit time integration technique based on the CVODE.

The model has been applied to various cases across multiple scales. The test case of pollutant transport in a square cavity shows the model can predict advection of pollutant by shallow water flow very well. Application of the model in a microscale pollutant transport following dam break compared the effects of advection and dispersion on pollutant transport, and show the advantage of the model in that the implicit treatment of the diffusion term makes it stable and its time step is not restricted by the Peclet number. The model is further applied to a mesoscale experiment about pollutant transport in Galveston Bay. This test case shows that the model is very stable and robust in simulating the mesoscale flow dynamics and pollutant transport driven by storm surge. It also indicates that the storm surge caused by the Hurricane Ike significantly extended the polluted area.

#### References

- [1] Murillo J, Burguete J, Brufau P, García-Navarro P. Coupling between shallow water and solute flow equations: analysis and management of source terms in 2D. *International Journal for Numerical Methods in Fluids* 2005; **49** (3): 267-99.
- [2] Katopodes N, Strelkoff T. Computing two-dimensional dam-break flood waves. *Journal of the Hydraulics Division, ASCE* 1978; **104**: 1269-88.
- [3] Molls T, Chaudhry MH. Depth averaged open channel flow model. *Journal of Hydraulic Engineering* 1995; **121**: 453-65.
- [4] Toro EF. *Shock-capturing Methods for Free-surface Shallow Flows*. John Wiley & Sons: Chichester; 2001
- [5] Sleigh PA, Berzins M, Gaskell OH, Wright NG. An unstructured finite-volume algorithm for predicting flow in rivers and estuaries. *Computers and Fluids* 1998; **27** (4): 479-508.
- [6] Horritt MS. Calibration and validation of a 2-dimensional finite element flood flow model using satellite radar imagery. *Water Resources Research* 2000; **36** (11): 3279-91.
- [7] Loukili Y, Soulaïmani A. Numerical Tracking of Shallow Water Waves by the Unstructured Finite Volume WAF Approximation. *International Journal for Computational Methods in Engineering Science and Mechanics* 2007. **8** (2): 75-88.
- [8] Harten A, Lax PD, van Leer B. On upstream differencing and Godunov-type schemes for hyperbolic conservation laws. *SIAM Rev.* 1983; **25** (1): 35-61.
- [9] Toro EF. Riemann problems and the WAF method for solving the two-dimensional shallow water equations. *Philos. Trans. R. Soc. London, Ser. A* 1992; **338**: 43-68.
- [10] Zoppou C, Roberts S. Catastrophic collapse of water supply reservoirs in urban areas. *Journal of Hydraulic Engineering* 1999; **125**: 686-95.

- [11] Osher S, Solomon F. Upwind difference schemes for hyperbolic conservation laws. *Math. Comput.* 1982; **38**: 339-74.
- [12] Jawahar P, Kamath H. A high-resolution procedure for Euler and Navier-Stokes computations on unstructured grids. *Journal of Computational Physics* 2000; **164**: 165-203.
- [13] Tan WY. *Shallow Water Hydrodynamics*, Elsevier, New York; 1992.
- [14] Liggett, JA. *Fluid Mechanics*, McGraw-Hill; 1994.
- [15] Shewchuk JR. *Delaunay refinement mesh generation*, PhD Thesis, Carnegie Mellon University; 1997.
- [16] Li S, Duffy CJ. Fully coupled approach to modeling shallow water flow, sediment transport, and bed evolution in rivers, *Water Resour. Res.* 2011; **47**: W03508, doi:10.1029/2010WR009751.
- [17] Bermudez A, Vázquez-Cendón ME. Upwind methods for hyperbolic conservation laws with source terms. *Computers and Fluids*, 1994; **23 (8)**:1049-71.
- [18] Bermudez A, Dervieux A, Desideri JA, Vazquez ME. Upwind schemes for the two-dimensional shallow water equations with variable depth using unstructured meshes. *Comput. Meth. Appl. Mech. Eng.* 1998; **155**: 49-72.
- [19] LeVeque RJ. Balancing source terms and flux gradients in high resolution Godunov methods, *J Comput Phys* 1998; **146**: 346-65.
- [20] Zhou JG, Causon DM, Mingham CG, Ingram DM. The Surface Gradient Method for the Treatment of Source Terms in the Shallow-Water Equations. *J Comput Phys* 2001; **168**: 1-25.
- [21] Bradford SF, Sanders BF. Finite-volume model for shallow-water flooding of arbitrary topography. *Journal of Hydraulic Engineering* 2002; **128**: 289-98
- [22] Delis AI. Improved application of the HLLC Riemann solver for the shallow water equations with source terms. *Commun. Numer. Meth. Eng.* 2003; **19**:59-83.
- [23] Hindmarsh AC, Serban R. User Documentation for cvode v2.3.0. Center for Applied Scientific Computing Lawrence Livermore National Laboratory, *UCRL-SM-208108*; 2005.
- [24] Shu CW, Osher S. Efficient implementation of essentially non-oscillatory shock capturing schemes. *J. Comput. Phys.* 1988; **77**: 439-71.
- [25] Komatsu T, Ohgushi K, Asai K. Refined numerical scheme for advective transport in diffusion simulation. *J. Hydraulic Eng.* 1997; **123**: 41–50.
- [26] Benkhaldoun F, Elmahi I, Seaid M. Well-balanced finite volume schemes for pollutant transport by shallow water equations on unstructured meshes. *Journal of Computational Physics* 2007; **226**: 180-203.
- [27] Aizinger V., Dawson C. A discontinuous Galerkin method for two-dimensional flow and transport in shallow water. *Advances in Water Resources* 2002; **25**: 67-84.